Bifurcations and complete chaos for the diamagnetic Kepler problem

Kai T. Hansen*
Fakultät für Physik, Universität Freiburg, Hermann-Herder-Strasse 3, D-79104 Freiburg, Germany
(Received 8 November 1994)

We describe the structure of bifurcations in the unbounded classical diamagnetic Kepler problem. We conjecture that this system does not have any stable orbits and that the nonwandering set is described by a complete trinary symbolic dynamics for scaled energies larger than $\epsilon_c = 0.328\,782\ldots$.

PACS number(s): 05.45.+b, 32.60.+i

The problem of a charged particle moving in a combined attracting electrical Coloumb field and a strong homogeneous magnetic field is a simple system showing complicated chaotic behavior. The corresponding quantum mechanical problem is a hydrogen atom in a strong magnetic field. This system is called the *diamagnetic Kepler problem* (DKP) and in the past decade this problem has been much investigated both classically and quantum mechanically in theoretical and experimental studies. Review articles by Friedrich and Wintgen [1] and Hasegawa *et al.* [2] yield good introductions to this problem. One interesting result of this research is an astonishing relation between the classical and the quantum mechanical systems, where the quantum mechanical energy levels analyzed in a proper way reflect the periodic orbits existing in the classical system. Most of these results have been on the bounded system with negative energy such that the electron cannot escape. We report here some numerical results concerning the classical orbits in the DKP with a positive energy, where quantum mechanically the atom can ionize. We also give some remarks on the implications for the quantum mechanical systems from the results obtained here.

The diamagnetic Kepler problem with zero angular momentum is given by the Hamiltonian

$$H = p^2/2m_e - e^2/r + \frac{1}{2}m_e\omega^2(x^2+y^2). \tag{1}$$

Using suitably scaled variables and semiparabolic coordinates this problem can be turned into the study of the Hamiltonian [1, 2]

$$h = \frac{1}{2}p_\nu^2 + \frac{1}{2}p_\mu^2 - \epsilon(\nu^2+\mu^2) + \frac{1}{8}\nu^2\mu^2(\nu^2+\mu^2) \equiv 2 \tag{2}$$

at the fixed "pseudoenergy" 2 and with a scaled energy $\epsilon = E\gamma^{-2/3}$ depending on both the energy E and the strength of the magnetic field γ. We consider the scaled energy ϵ to be a parameter when we investigate the classical trajectories.

The Hamiltonian (2) has a rather complicated bifurcation structure for $\epsilon < 0$ and there is not any known symbolic dynamics description of the orbits. For $\epsilon \geq 0$ it has been proposed by Eckhardt and Wintgen [3] that the orbits may be described by the same symbols as the four-disk system [4] and that this four-disk symbolic dynamics for periodic orbits (cycles) can be obtained in the DKP by finding self-conjugate points. The four-disk system consists of a point particle moving freely on a two-dimensional plane and bouncing elastically off the boundaries of four disks in the plane. The four disks have radius 1 with the disk centers at the four points $(\pm r/2, \pm r/2)$ in the (ν, μ) plane. The center-center distance r is the parameter for the four-disk problem.

For the Hamiltonian system with the smooth potential $V(x,y) = (xy)^{2/a}$ it has been argued that the bifurcations are very similar in this smooth potential and in the four-disk billiard [6–8]. This seems to be true also for the DKP with positive ϵ and this yields a method to determine stable orbits and to find the parameter value where the repellor is a complete Cantor set. We can then show that there are no elliptic orbits above a critical energy ϵ_c, which has to be determined numerically.

In a dispersing billiard system the singular orbits which define the pruning front [9–11] are the orbits tangent to the boundary. The pruning front determines which orbits are admissible in the system and all bifurcations take place on this pruning front. In the four-disk billiard we obtain a symbolic dynamics description by enumerating the disks clockwise and the symbolic dynamics of a trajectory is given by a string $\ldots s_{-1}s_0s_1s_2\ldots$ where s_t is the label of the disk the particle bounces off at the integer time t. Other alphabets can be defined from this basic alphabet [4, 11]. The first orbits, which become forbidden in the four-disk system as the distance between the disk centers decreases to a critical distance $r_c = 2.2046\ldots$, are the heteroclinic orbits $\overline{14}\ \overline{21}$ and $\overline{14}\,1\,\overline{21}$ (a line above a string denotes an infinite repetition of this string $\overline{14}\ \overline{21} = \ldots 141414212121\ldots$) and orbits symmetric to these [10, 11]. These orbits are the corners of the two-dimensional Cantor set of nonwandering [5] (not escaping) orbits in phase space and are the first to become nonadmissible in a symmetric system. We show below that these heteroclinic orbits also are the

*Also at Physics Department, University of Oslo, Box 1048, Blindern, N-0316 Oslo, Norway. Electronic address: k.t.hansen@fys.uio.no

corners of the nonwandering Cantor set for the complete chaotic DKP.

The idea that singular orbits determine the set of admissible orbits can be carried over from the hard billiard systems to the soft potential systems. One then has to determine the orbits in the smooth system which correspond to the tangential orbits in the billiard. A second way to view the analogy between hard and soft systems is to draw the manifold structures in a Poincaré map. This yields a simpler and maybe more familiar picture, but the symbolic dynamics and physical interpretation are more difficult to get from this point of view. We will discuss here both approaches to the problem.

There does not exist a steep wall in the smooth system as it does in the billiard system and consequently no direct way to find a "tangent" orbit, but the singular orbits in the billiards have another property for which we can find an analog to in smooth systems and we will apply this to determine the singular orbits. Assume that there exists a singular orbit tangent to the boundary in the four-disk system. Then choose a second orbit close to the singular orbit at the tangent point but a finite distance δ away from the boundary and such that this second orbit bounces off different disks than the first orbit after some time. This second orbit will then have a different symbolic description from the singular orbit. Then there will also exist a third orbit bouncing off the boundary near the tangent point of the first orbit with some finite angle ϕ with a symbolic description identical to the second orbit both in the future and in the past. We can define the singular orbit as an orbit with extremum future and past trajectories since the two different neighbor trajectories have identical symbolic dynamics in the past and the future. In a well ordered symbolic alphabet [11] this yields a extremum symbolic value and in the configuration space the two neighbor orbits moves on the same side of the singular trajectory. This new definition of singular orbits as extremum orbits can be applied also in the case of a smooth potential. The set of all singular orbits is a one-parameter family of orbits in the four-disk system and this seems to be true also for the smooth Hamiltonian (2) in the DKP.

In the following, for simplicity, we mostly discuss the singular orbit normal to the diagonal $\mu = \nu$. It is clear from the symmetry of the problem that there will exist such a singular orbit and as for the four-disk system this singular orbit becomes the heteroclinic orbit $\overline{14}\ \overline{21}$ at the critical parameter value ϵ_c. Then there is no pruning for $\epsilon > \epsilon_c$. The singular orbit on the $\nu_0 = \mu_0$ line can be found numerically by scanning a one-dimensional starting point $\nu_0 = \mu_0$ keeping $p_{\nu_0} = -p_{\mu_0}$, while for other nonsymmetric singular orbits one has to scan both the starting points and the direction of the velocity.

Figure 1 shows a segment of the singular orbit for the scaled energy $\epsilon = 0$ from the starting point $\nu_0 = \mu_0 = 0.816$ together with two neighboring orbits starting parallel with this at $\nu_0 = \mu_0 = 0.716$ (dashed curve) and at $\nu_0 = \mu_0 = 0.916$ (dotted curve). Both the two neighbor trajectories are on the same side of the singular trajectory after some transient time both in the future and in the past. There are no trajectories on the other (forbidden) side of the singular trajectory both in the past and in the future. There may be orbits on this forbidden side in the past *or* in the future, but not both in the past and in the future.

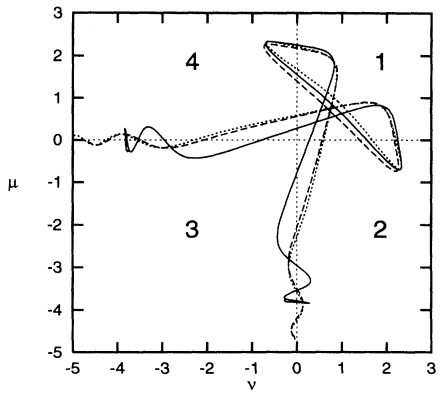

FIG. 1. Singular orbit and two neighbor orbits for $\epsilon = 0$ in the diamagnetic Kepler problem (DKP). The numbers indicate the symbols of the four-disk system.

The orbit starting at $\nu_0 = \mu_0 = 0.716$ corresponds to the orbit in the billiard system which passes the boundary of disk 1 at some distance δ, while the orbit starting at $\nu_0 = \mu_0 = 0.916$ corresponds to the billiard orbit bouncing off the boundary of disk 1 with some angle ϕ. By drawing the orbits in configuration space we can determine the singular orbit and we find that the singular orbit for $\epsilon = 0$ starts at $\nu_0 = \mu_0 = 0.816\,617\,9\ldots$.

The singular orbit in Fig. 1 shows that there cannot exist any orbit described by a symbol string containing a substring ——414212—— or ——4141212—— for $\epsilon = 0$. This orbit would be on the forbidden side of the singular trajectory. One forbidden periodic orbit is then $\overline{41412121}$. Since the symmetric singular orbit for $\epsilon = 0$ numerically appears to be nonperiodic, there is an infinite number of forbidden symmetric substrings of increasing length determined by this singular orbit.

To determine all forbidden substrings one also has to determine the nonsymmetric singular orbits. One example of a nonsymmetric singular orbit is drawn in Fig. 2. Here we have numerically determined a trajec-

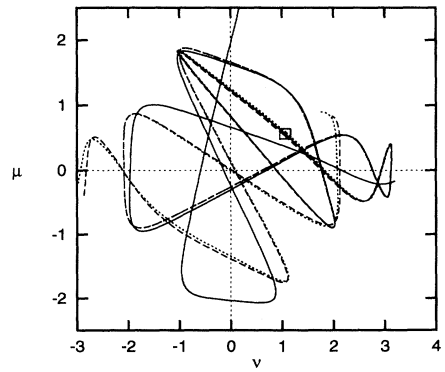

FIG. 2. Nonsymmetric singular orbit and two neighbor orbits for $\epsilon = 0$.

tory with extremum future and past compared to orbits starting parallel to it. This orbit starts at $\nu_0 = 0.561\,66$, $\mu_0 = 1.561\,66$, and with $p_{\nu_0}/p_{\mu_0} = -\tan(0.605)$. From Fig. 2 we can read off that, for example, the orbits containing a substring ——1421212—— or ——14121212—— are forbidden. This is a slightly different rule from that we got from Fig. 1. All the rules obtained from all singular orbits yield all rules which determine the forbidden orbits in the system.

As ϵ increases, the singular orbits will change and for some values of ϵ, a singular orbit may return close to the starting point with a similar direction. When the singular orbit returns it implies that we get a stable periodic orbit. Since orbits near the singular orbit do not diverge but approach each other around the starting point of the singular orbit, this gives rise to stability for periodic orbits. One example of this is given in Fig. 3 for the scaled energy $\epsilon = 0.1113$, where the singular orbit is found at $\mu_0 = 0.8617$. The stable cycle existing here is $\overline{41412121}$. This cycle we found above to be inadmissible at $\epsilon = 0$ and it will be admissible for all $\epsilon > 0.1113$. The cycle is in the center of a stable island and it is not directly a forbidden and legal side of the singular orbit here, but the admissibility is determined by the rotation number of the elliptic orbits. The nearby orbits drawn in Fig. 3 start outside the stable island.

Inserted in Fig. 3 is a Poincaré map showing (ν, p_ν) when the trajectory crosses the $\nu = \mu$ line for five different starting points close to the singular trajectory $(0.855 < \nu < 0.869, 1.4354 < p_\nu < 1.4375)$. We find here the usual Hamiltonian structure of Kol'mogorov-Arnol'd-Moser (KAM) curves and resonances. We conjecture that all the periodic and quasiperiodic orbits within the stable island can be given a unique symbolic coding by adiabatically following the trajectories into the completely chaotic region $\epsilon > \epsilon_c$ and that they belong to one bifurcation family of the four-disk system; see Ref. [8]. The symbolic dynamics of these orbits are given as a string $\ldots 414s_{-1}212s_0414s_1212\ldots$, where s_t is the symbol 1 or no symbol. All the cycles symmetric across the $\mu = \nu$ line are stable when they are on the symmetric singular orbit and hyperbolic otherwise.

We will now try to find the parameter value ϵ_c where the singular orbit escapes directly to $\nu \to \infty$ in the future direction and to $\mu \to \infty$ in the past direction without ever returning. It is not trivial, however, to decide when a trajectory leaves to infinity in this system because for an arbitrary large value of ν (or of μ) there exist orbits coming from and returning to the $\nu = 0$ line ($\mu = 0$ line). One example of this is an orbit crossing the ν-axis with $p_\nu = 0$ for a large value of ν. This trajectory will cross the $\nu = 0$ line both in the future and in the past and may be a nonescaping trajectory.

Numerically it turns out that it is possible to distinguish escaping and nonescaping trajectories by plotting the Poincaré map (μ, p_μ) for each crossing of the μ axis with $p_\mu > 0$ (correspondingly for ν). Escaping trajectories yield points approximately along or above a straight line $p_\mu = a\mu + b$ with $a > 0$. Returning trajectories will yield points along an oval shaped curve in the Poincaré map (μ, p_μ). We can then distinguish between escaping and nonescaping trajectories by following the trajectory a reasonably short time.

Figure 4 shows the Poincaré map for three orbits starting at $\mu = \nu = 0.75$ (diamonds), 0.9 (pluses), and 1.05 (squares), $p_{\nu_0} = -p_{\mu_0}$, for the scaled energy $\epsilon = 0.335$. The trajectory from 0.9 escapes directly while the other two return to the $\mu = 0$ line (but may escape at some later time). The escaping trajectory is drawn in configuration space (ν, μ) in Fig. 5. The orbit simply comes in from $\mu = \infty$ and continues out to $\nu = \infty$. When the symmetric singular orbit escapes directly there is no pruning left in the system and we will have a complete Cantor set repellor. Other nonsymmetric singular orbits will for some $\epsilon < \epsilon_c$ escape to infinity either in the future or in the past. There will not be any stable cycles since stable

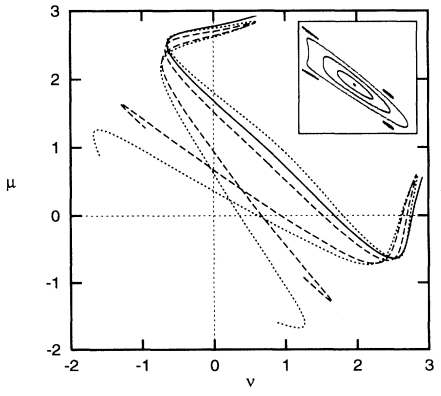

FIG. 3. Singular orbit and two neighbor orbits for $\epsilon = 0.1113$ where the singular orbit is a stable periodic orbit. Inserted is a Poincaré map (μ, ϕ) for $\nu = \mu$ showing KAM curves.

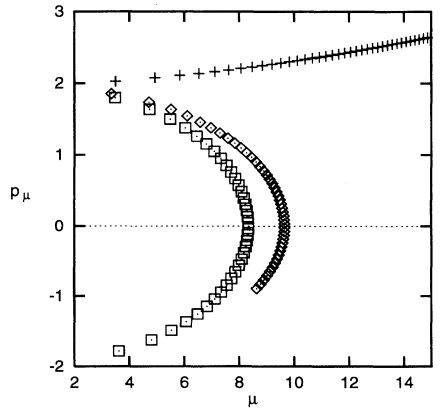

FIG. 4. Poincaré map (μ, p_ν) for $\nu = 0$ of three trajectories from $\nu_0 = \mu_0, p_{\nu_0} = -p_{\mu_0}$ showing that there is one trajectory escaping directly, yielding a completely chaotic system.

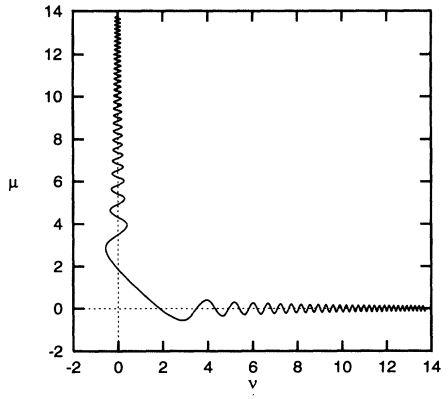

FIG. 5. The orbit yielding the escaping trajectory in the Poincaré map in Fig. 4, arriving from $\mu = \infty$ and continuing directly to $\nu = \infty$.

cycles only appear near a nonescaping singular orbit.

There is one orbit missing from the Cantor set and this is the cycle $\overline{12}$, which is only approached in the $\nu \to \infty$ limit. Orbits approaching this cycle, for example, $\overline{34(12)^n}$, $n \to \infty$, are then not bounded by a maximum value of ν, but they are unstable.

Numerically we determine the critical parameter value to be $\epsilon_c = 0.328\,782\ldots$.

A different way to discuss this problem is to draw the manifold structures in a Poincaré plane. In this way we can visualize how the stable and the unstable manifolds cross each other with a finite angle for $\epsilon > \epsilon_c$. When all stable and unstable manifolds cross with a finite angle (no tangencies), then the system is hyperbolic. In Fig. 6(a) we have drawn all starting points in a Poincaré plane which have not escaped after some fixed integration time T for the scaled energy $\epsilon = 0.35$. We have chosen the Poincaré plane where the trajectory crosses the $\nu = \mu$ line from $\nu < \mu$ to $\nu > \mu$ with the coordinates (μ, ϕ), where ϕ is the angle of the trajectory with the ν axis; $p_\mu/p_\nu = \tan\phi$. This Poincaré plane is finite with $-3\pi/4 < \phi < \pi/4$ and $-\mu_{\max} < \mu < \mu_{\max}$, where $\mu_{\max}(\epsilon)$ is found analytically from (2). To determine if a trajectory has escaped we use the idea from Fig. 4 that an orbit escapes if the value of p_μ (p_ν) increases from one to the next crossing of the μ axis (ν axis). The stable manifolds W^s are included in the set of nonescaping trajectories and for a sufficiently large T this yields a good picture of W^s. All points on the border curve, $\phi = -3\pi/4$, $\phi = \pi/4$, or $\mu = \pm\mu_{\max}$ in the Poincaré map, correspond to the hyperbolic period two cycle $\overline{13}$. The structure close to the border can be mapped into the structure in the middle of the Poincaré plane (close to the period-two cycle $\overline{24}$) by, e.g., $\nu \to -\nu$. Below we also draw the manifolds in a Poincaré map that does not have this strange border but which is, on the other hand, infinite.

The unstable manifolds W^u are symmetric to W^s with respect to the line $\phi = -\pi/4$. Both W^u and W^s are drawn in Fig. 6(b) and the crossing points between the W^u and W^s curves yield the nonwandering set. We find here that all the crossings between the curves of W^u and W^s have a finite angle and consequently all orbits are hyperbolic. In Fig. 6 it is simple to recognize a three-interval Cantor set structure of the manifolds. It is slightly more complicated to recognize this at the edges because the border curve corresponds to one unstable cycle and here we have only one-half of the Cantor set. This only depends on our choice of Poincaré map and does not give any real problems.

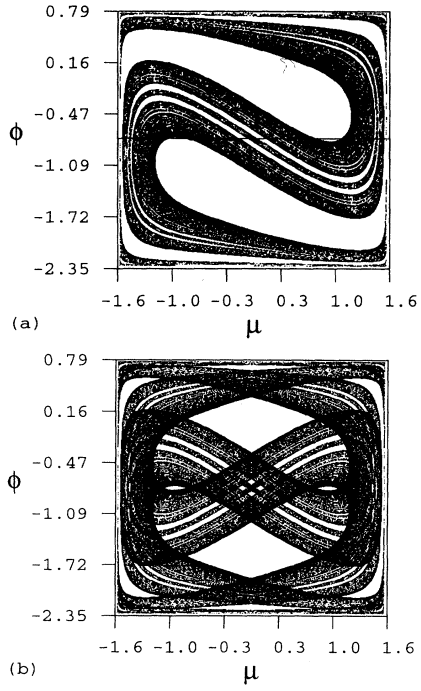

FIG. 6. Manifolds of the DKP in the Poincaré map (μ, ϕ) for $\epsilon = 0.35$: (a) W^s and (b) W^s and W^u.

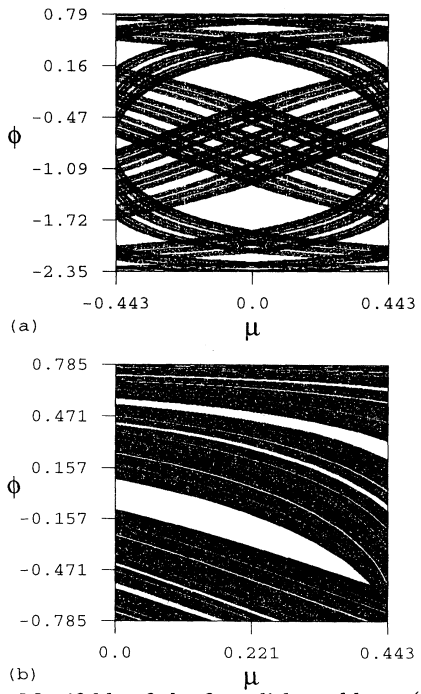

FIG. 7. Manifolds of the four-disk problem: (a) W^s and W^u for $r = 2.3$ and (b) W^s for $r = 2.06$.

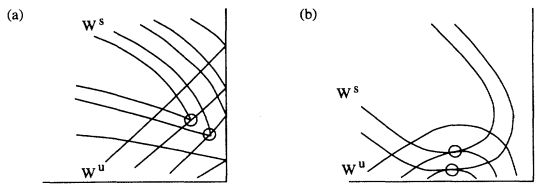

FIG. 8. Sketch of the structure of homoclinic tangencies in (a) the four-disk system and (b) the DKP.

These figures give a similar structure of manifolds as the manifold structure one can find for a four-disk system. The stable and the unstable manifolds for the four-disk system in a corresponding Poincaré map are drawn in Fig. 7. In Fig. 7(a) both the stable and the unstable manifolds are drawn for the disk-disk distance $r = 2.35$, $-3\pi/4 < \phi < \pi/4$, $1/\sqrt{2} - r/2 < \mu < r/2 - 1/\sqrt{2}$. This yields nice trinary Cantor sets as crossing points between W^u and W^s in the same way as in Fig. 6(b). The main structure is exactly the same in the billiard system [Fig. 7(a)] and in the smooth system [Fig. 6(b)]. The important difference is that in the DKP all folds smoothly connect for large values of $|\mu|$, while for the four-disk system the manifolds are discontinuous at the line $\mu = \mu_{\max}$. This discontinuous jump from ϕ to $\pi/2-\phi$ for the folds of the four-disk system is, loosely speaking, for the DKP glued together and the folds smoothly connect at the line $\phi = -\pi/4$. The two drawings yield the same number of crossings between W^u and W^s.

We can also compare the pruned systems for the DKP ($\epsilon < \epsilon_c$) and the four-disk system ($r < r_c$) in this Poincaré plane. In Fig. 7(b) the stable manifold W^s for the four-disk system is drawn for the disk distance $r = 2.06$. Here we have drawn one-quarter of the full phase space $-\pi/4 < \phi < \pi/4$, $0 < \mu < r/2 - 1/\sqrt{2}$. We find that the largest white area, which corresponds to orbits escaping without ever returning, no longer reaches the $\phi = -\pi/4$ line as it does in Fig. 7(a). Some crossings between the stable and the unstable manifolds existing for $r = 2.35$ are here lost and then also an infinite number of periodic orbits are inadmissible. A sketch of the manifold structure is given in Fig. 8(a). The points where a cusp of

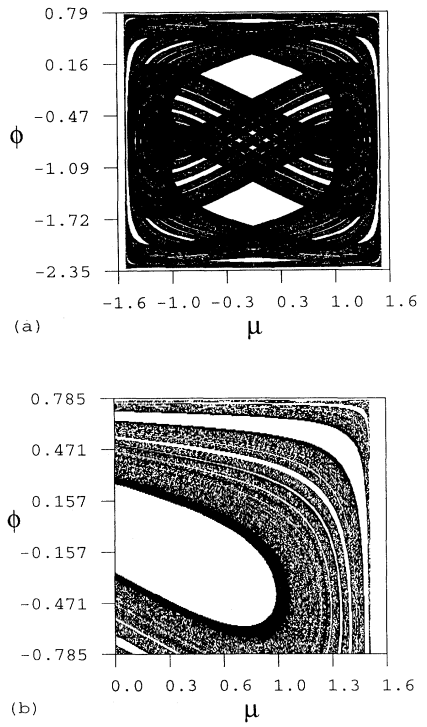

FIG. 9. Manifolds of the DKP for $\epsilon = 0.2$: (a) W^s and W^u and (b) W^s.

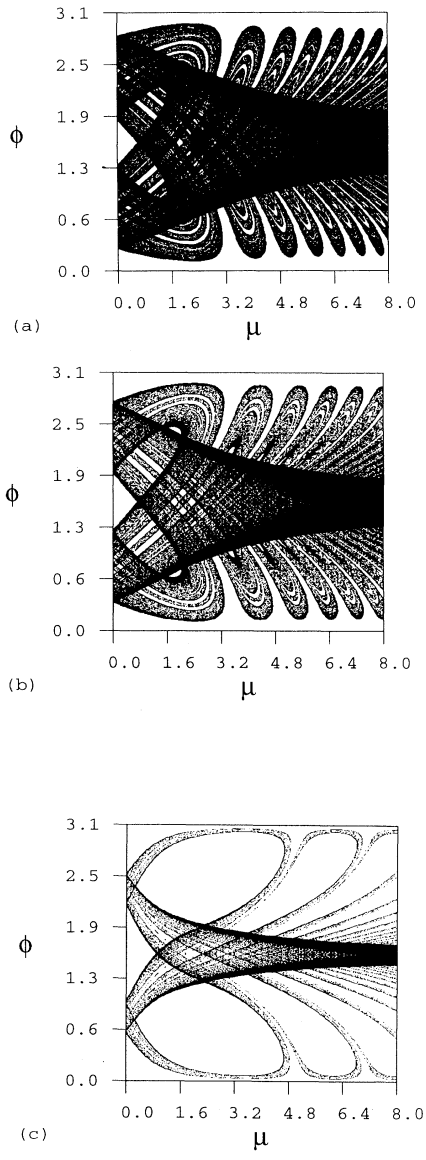

FIG. 10. Manifolds of the DKP W^s and W^u in the Poincaré map (μ, ϕ) for $\nu = 0$ for (a) $\epsilon = 0.2$, (b) $\epsilon = 0.35$, and (c) $\epsilon = 2.0$

the stable manifold touch a fold of the unstable manifold are marked with circles. These singular points are exactly the images of the tangent orbits. Moving the disks slightly closer to each other makes the homoclinic orbit at this touching point inadmissible. This is the analog in a billiard to the point called a homoclinic tangency for smooth dynamical systems. For simplicity we also denote this point a homoclinic tangency. One important remark here is that the homoclinic tangencies indicated in Fig. 8(a) are the primary tangencies and all other tangencies in other part of the phase space are images of these. The different primary tangencies are associated with different tangent orbits in the billiard. There is a one to one correspondence between a primary homoclinic tangency and singular orbits in the billiard. The homoclinic tangencies can be used to define the pruning front.

In Fig. 9 manifolds are drawn for the diamagnetic Kepler problem with $\epsilon = 0.2 < \epsilon_c$. In Fig. 9(a) both the stable and the unstable manifolds are drawn, while in Fig. 9(b) only the stable manifolds are drawn in one-quarter of the phase space $0 < \mu < \mu_{\max}$, $-\pi/4 < \phi < \pi/4$. Comparing Fig. 9(b) with Fig. 7(b) we find a very similar structure. The main difference is that the manifolds in Fig. 9(b) are smooth, while in Fig. 7(b) the bending points are sharp. For the DKP we have homoclinic tangencies where the unstable and the stable manifolds are tangents and for an infinitesimal smaller parameter ϵ these homoclinic orbits are inadmissible. The structure of the homoclinic tangencies is sketched in Fig. 8(b). As for the four-disk system we have a one-parameter family of primary homoclinic tangencies, each associated with a singular orbit. The situation in the soft potential is slightly more complicated because a stable orbit creates a stable island in the neighborhood of a homoclinic tangency. One example of such an island is the orbit in Fig. 3. One way to numerically determine the pruning front is to draw the unstable and the stable manifolds and determine the set of primary homoclinic tangencies. This can also be done for the closed system ($\epsilon = 0$) by using the manifolds of a hyperbolic periodic orbit.

To further illustrate the hyperbolicity for this system, we draw the manifolds in a different Poincaré map where the trajectory crosses the μ axis with ν changing from negative to positive. The manifolds in Fig. 9(b) for the DKP at $\epsilon = 0.20$ are drawn in Fig. 10(a). Here there are a number of homoclinic tangencies giving rise to pruning and stable orbits. The manifolds in Fig. 6(b) for the hyperbolic map at $\epsilon = 0.35$ are drawn in Fig. 10(b). Here we find that the manifolds always cross with a finite angle and there are no tangencies. In Fig. 10(c) the same manifolds are drawn for a large scaled energy $\epsilon = 2.0$. Here we find that the same Cantor set of crossings between the stable and the unstable manifolds, but the Cantor set is thinner. No new nonescaping orbits are created when ϵ increases because the manifolds only move closer to the $\phi = 0$ and $\phi = \pi$ lines. It is reasonable to conjecture that no new orbits are created as ϵ increases further and the nonwandering set of the DKP has the same topological structure for all $\epsilon > \epsilon_c$.

An advantage of this Poincaré map is that we avoid the complicated border orbit we had in Figs. 6 and 9 and it is easy to see that no new orbits are created as ϵ increases. The disadvantage is that the plane is unbounded and as μ increases we get more and more copies of the foliations. Each new copy has only one more bounce than the presiding one and does not yield any new information.

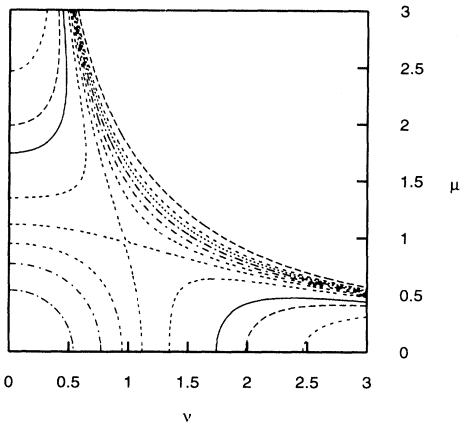

FIG. 11. Potential at the critical scaled energy $\epsilon_c = 0.328\,782$.

In Fig. 11 equipotential lines are drawn at ϵ_c. In addition to the hyperbolalike curves also existing at $\epsilon = 0$, there are saddle points and a "hill" at the origin. These latter structures turn out not to give rise to any new singular orbits and stable cycles. The potential at the origin is 0 and trajectories cannot turn there. The hill structure only adds instability to the Cantor set repellor.

In quantum mechanical calculations [12–14] one has found resonances and some with a very narrow width. In quantum mechanical calculations these appear because of the cancellation of some matrix elements. Semiclassically these can be associated with stable orbits such as the one in Fig. 3. When we have a pure hyperbolic classical system ($\epsilon > \epsilon_c$) we can predict that a quantum mechanical cross section (for ϵ constant) does not have any narrow width resonances. All the other resonances can be calculated by periodic orbit expansion of the unstable periodic orbits and work on this continues.

The DKP with negative scaled energy has a more complicated structure and more mechanisms giving stable orbits. For small negative energies the pruning front orbits discussed above still exist as a part of the complete pruning mechanism.

From the results presented above it seems that the Hamiltonian (2) with $\epsilon > \epsilon_c$ is a completely chaotic scattering smooth system, without any singularities and where the set of all periodic orbits (and the nonwandering set) is unbounded in the configuration space. To the authors knowledge there are no earlier examples of this in the literature.

The author wishes to express his gratitude to Dieter Wintgen for the few interesting discussions time allowed. The author thanks colleagues in Copenhagen and Freiburg for helpful discussions. The author is grateful to the Alexander von Humboldt foundation for financial support.

[1] H. Friedrich and D. Wintgen, Phys. Rep. **183**, 37 (1989).
[2] H. Hasegawa, M. Robnik, and G. Wunner, Prog. Theor. Phys. Suppl. **98**, 198 (1989).
[3] B. Eckhardt and D. Wintgen, J. Phys. A **24**, 4335 (1991).
[4] P. Cvitanović and B. Eckhardt, Nonlinearity **6**, 277 (1993).
[5] S. Smale, Bull. Am. Math. Soc. **73**, 747 (1967).
[6] K.T. Hansen, Ph.D. thesis, University of Oslo, 1993.
[7] P. Dahlqvist and G. Russberg, J. Phys. A **24**, 4763 (1991).
[8] K.T. Hansen, Nonlinearity **6**, 771 (1993).
[9] P. Cvitanović, G.H. Gunaratne, and I. Procaccia, Phys. Rev. A **38**, 1503 (1988).
[10] K.T. Hansen, CHAOS **2**, 71 (1992).
[11] K.T. Hansen, Nonlinearity **6**, 753 (1993)
[12] H. Friedrich and M. Chu, Phys. Rev. A **28**, 1423 (1983).
[13] H. Friedrich and D. Wintgen, Phys. Rev. A **31**, 3964 (1985).
[14] D. Delande, A. Bommier, and J.C. Gay, Phys. Rev. Lett. **66**, 141 (1991).